ISSN 1063-7745, Crystallography Reports, 2016, Vol. 61, No. 4, pp. 558–565. © Pleiades Publishing, Inc., 2016.
Original Russian Text © E.S. Smirnova, O.A. Alekseeva, A.P. Dudka, I.A. Verin, V.V. Artemov, L.N. Bezmaternykh, I.A. Gudim, K.V. Frolov, I.S. Lyubutin, 2016, published in Kristallografiya, 2016, Vol. 61, No. 4, pp. 535–542.

STRUCTURE OF INORGANIC COMPOUNDS

Structure of $Gd_{0.95}Bi_{0.05}Fe_3(BO_3)_4$ Single Crystals at 293 and 90 K

E. S. Smirnova[a], O. A. Alekseeva[a], A. P. Dudka[a], I. A. Verin[a], V. V. Artemov[a], L. N. Bezmaternykh[b], I. A. Gudim[b], K. V. Frolov[a], and I. S. Lyubutin[a]

[a] *Shubnikov Institute of Crystallography, Russian Academy of Sciences, Leninskii pr. 59, Moscow, 119333 Russia*
[b] *Kirensky Institute of Physics, Siberian Branch, Russian Academy of Sciences, Akademgorodok 50, str. 38, Krasnoyarsk, 660036 Russia*
e-mail: olalex@ns.crys.ras.ru

Received December 24, 2015

Abstract—The structure of $GdFe_3(BO_3)_4$ single crystals has been studied by X-ray diffraction at 293 and 90 K. The crystals are grown from a flux in the $Bi_2Mo_3O_{12}$–B_2O_3–Li_2MoO_4–Gd_2O_3–Fe_2O_3 system. The results of chemical analysis and structural study show that these crystals contain bismuth as an impurity. It is found that bismuth atoms are located at gadolinium sites in the structure. A decrease in the temperature is accompanied by a lowering of the symmetry from sp. gr. $R32$ (at 293 K) to sp. gr. $P3_121$ (at 90 K). The presence of two types of iron chains with different geometries at 90 K promotes a change in the magnetic properties of these crystals with a decrease in the temperature.

DOI: 10.1134/S1063774516040192

INTRODUCTION

New multiferroic compounds and the nature of magnetoelectric effects observed in these compounds have received considerable attention from researchers due to a broad range of possible applications of such materials. The family of rare earth borates $RM_3(BO_3)_4$ (R = Y, La–Lu, Bi, In; M = Al, Sc, Fe, Ga, Cr) belongs to magnetoelectric materials, although these compounds have initially attracted interest due to non-linear-optical and laser properties. Rare earth iron borates $RFe_3(BO_3)_4$ are the least studied compounds of this family. They are assigned to multiferroics due to spontaneous electric polarization, as well as magnetoelectric and magnetoelastic properties. The diverse properties of iron borates are attributed to the presence of two magnetic subsystems formed by iron and rare earth ions [1, 2].

Compounds of the $RFe_3(BO_3)_4$ family were synthesized for the first time as polycrystalline samples for R = La, Nd, Sm–Ho, and Y [3]. Single crystals of $RFe_3(BO_3)_4$ can be grown by crystallization from Bi_2O_3-based [4], $Bi_2Mo_3O_{12}$-based [5], or $K_2Mo_3O_{10}$-based fluxes [6].

Crystals of the $RFe_3(BO_3)_4$ family undergo a first-order structural phase transition (PT) accompanied by a change in symmetry. At temperatures higher than the PT temperature, all crystals have a trigonal structure of the mineral huntite $CaMg_3(CO_3)_4$ described by sp. gr. $R32$ [1, 7]. A characteristic feature of the iron borate structure is the presence of independent helicoidal chains of FeO_6 octahedra running along the c axis. The chains are linked by triangular BO_3 groups and distorted RO_6 trigonal prisms.

In compounds containing rare earth metals with a large ionic radius (R = La, Ce, Pr, Nd, Sm), the above-described structure remains unchanged down to 2.7 K, whereas in compounds containing ions with a smaller radius (R = Eu, Gd, Tb, Dy, Ho, Er, Y) the PT temperature increases from 88 to 450 K with a decrease in the ionic radius [1, 2, 8–11].

The structural PT was found for the first time in gadolinium iron borate $GdFe_3(BO_3)_4$ near 155 K by heat-capacity measurements and Raman spectroscopy [12] and by measuring the temperature dependence of dielectric permeability [9]. Gadolinium iron borate $GdFe_3(BO_3)_4$ was found to undergo a series of magnetic, structural, optical, and electronic transitions induced by high pressures up to P = 60 GPa [13–16].

Despite the fact that a similar structural PT was later observed in many representatives of the $RFe_3(BO_3)_4$ family, the low-temperature crystal structures of most of these compounds were not determined. The crystal structures of high-symmetry phases of many representative of this family are also not available in crystallographic databases. The following single crystals of the $RFe_3(BO_3)_4$ family have been studied by X-ray diffraction: $(Nd_{0.5}Bi_{0.5})Fe_3(BO_3)_4$ [17], $LaFe_3(BO_3)_4$, $NdFe_3(BO_3)_4$, and $(Y_{0.5}Bi_{0.5})Fe_3(BO_3)_4$ [4], $GdFe_3(BO_3)_4$ [18], and $ErFe_3(BO_3)_4$ [19].

In [18] the $GdFe_3(BO_3)_4$ single crystals, which were grown using a $K_2Mo_3O_{10}$-based flux, were studied

by X-ray diffraction at room temperature and at 90 K. At both temperatures the unit cell of the crystals was determined as trigonal. In the cited study, it was shown for the first time that the first-order PT is accompanied by a change in sp. gr. $R32 \rightarrow P3_121$. The transition to the low-symmetry space group gives rise to two nonequivalent sites of iron atoms that form helicoidal chains.

It should be noted that lowering the temperature was shown to lead to an increase in unit-cell parameters [18] ($a = 9.5203(6)$ Å, $c = 7.5439(5)$ Å at $T = 297$ K and $a = 9.5305(3)$ Å, $c = 7.5479(2)$ Å at $T = 90$ K), but this fact was not analyzed. However, a detailed investigation into the unit-cell parameters of $GdFe_3(BO_3)_4$ single crystals grown from a $BiMo_3O_{12}$–B_2O_3–Li_2MoO_4-based flux in the temperature range of 30–295 K [20] did not reveal this abnormality. Meanwhile, an increase in the unit-cell parameter c accompanied by a gradual decrease in the unit-cell volume and the unit-cell parameters a and b was observed at $T < 80$ K [20].

In order to reveal the relationship between the structure and magnetoelectric properties of iron borates, it is necessary to get accurate data on the unit-cell parameters and the geometry of the atomic arrangement in a wide temperature range. The character of exchange interaction between magnetic cations depends directly on crystal-chemical parameters such as interatomic distances, exchange bond angles, electronic states, and the sizes of atoms. For example, it is known that a strong dependence of the exchange interaction on the interatomic distance can lead to a change in the sign of interactions for some atoms [21].

Therefore, it is of interest to perform systematic structural studies of iron borate single crystals in a wide temperature range in order to establish the relationship between their physical properties and the characteristic features of the crystal structure.

The aim of the present study was to obtain complete and accurate data on the structure of $GdFe_3(BO_3)_4$ single crystals at different temperatures by means of high-precision X-ray diffraction.

EXPERIMENTAL

Single crystals of $GdFe_3(BO_3)_4$ were grown from a flux in the $Bi_2Mo_3O_{12}$–B_2O_3–Li_2MoO_4–Gd_2O_3–Fe_2O_3 system by a procedure described in [5]. The chemical composition of the compound was refined by energy-dispersive X-ray spectroscopy (EDS) using a FEI Quanta 200 3D Dual Beam scanning electron microscope equipped with an EDAX EDS system at an accelerating voltage of 5, 15, and 30 kV. It was shown that the crystals contain bismuth, which was attributed to the procedure used for the synthesis.

The most perfect single crystals were chosen for the X-ray diffraction study. The crystals were ground to a nearly spherical shape to facilitate absorption correction. The samples were subjected to preliminary X-ray diffraction analysis in order to select a single crystal characterized by the best X-ray diffraction peak profiles and the smallest difference in the intensities of symmetry-equivalent reflections.

In addition to the temperature scanning of the unit-cell parameters [20], the temperature dependence of the unit-cell parameters was measured on a CAD-4F Enraf-Nonius diffractometer equipped with a CryoJetHT low-temperature attachment (Oxford Instruments) controlled with a liquid-nitrogen open-flow cooler in a temperature range of 90–293 K with a step of 30 K. In the vicinity of the expected PT, the unit-cell parameters were measured with a step of 1–2 K. The measurements were performed taking into account the calibration of the CryoJetHT low-temperature attachment by a procedure described in [22]. A sharp decrease in the unit-cell parameters a and b near 155 K is indicative of the structural PT, which is consistent with the data measured on a Huber X-ray diffractometer equipped with a Displex DE-202 closed-cycle helium cryostat [20].

The complete X-ray diffraction data sets were collected on an Xcalibur S automated four-circle X-ray diffractometer equipped with a CCD area detector at 293 and 90 K. At 90 K (measured by a CryoJetHT temperature system), two sets of diffraction intensities were collected at different orientations of the sample at a high interplanar-spacing resolution. The repeated X-ray data collected allowed us to calibrate the diffractometer [23] and calculate an accurate absorption correction [24], resulting in a significantly larger number of independent reflections being included in the structure refinements based on the low-temperature data. The integration of diffraction peaks was performed using the CrysAlis program incorporated into the diffractometer software [25].

The unit-cell search for the crystal under study resulted in the choice of the trigonal unit cell with the parameters $a = 9.5554(1)$ Å, $c = 7.5768(1)$ Å at $T = 293$ K and $a = 9.5473(1)$ Å, $c = 7.5642(1)$ Å at $T = 90$ K. Therefore, it was found that, as opposed to the results published in [18], the unit-cell parameters regularly decrease with a decrease in the temperature. It should be noted that these data correlate well with the dependence obtained in [20] using a Huber-5042 diffractometer.

An analysis of systematic absences revealed sp. gr. $R32$ at 293 K and sp. gr. $P3_121$ at 90 K. A change in the space group is attributed to the structural PT observed at $T \sim 155$ K. Similar structures were determined in [18], which is also evidence of the first-order structural PT in gadolinium iron borate in the temperature range of 90–293 K [18, 20].

The structures were refined by the least-squares method using the Jana2006 program [26]. The extinction and Flack parameters were refined. In order to take into account extinction effects, the best

Table 1. Crystallographic parameters and the X-ray-data-collection and structure-refinement statistics for the compound $Gd_{0.95}Bi_{0.05}Fe_3(BO_3)_4$

Chemical formula	$Gd_{0.95}Bi_{0.05}Fe_3(BO_3)_4$	
Crystal system, sp. gr., Z	Trigonal, $R32$, 3	Trigonal, $P3_121$, 3
a, c, Å	9.5554(1), 7.5768(1)	9.5473(1), 7.5642(1)
V, Å^3	599.120(12)	597.111 (12)
D_x, g/cm^3	4.678	4.6937
Radiation; λ, Å	MoK_α; 0.71073	
μ, mm^{-1}	14.302	14.350
T, K	293	90
Diameter of the sample, mm	0.29	0.29
Diffractometer	Oxford Diffraction CCD	
Scanning mode	ω	
Absorption correction; T_{min}, T_{max}	Sphere; 0.0741, 0.1739	Sphere; 0.0736, 0.1733
θ_{max}, deg	73.81	74.05
h, k, l ranges	$-24 \leqslant h \leqslant 22$; $-23 \leqslant k \leqslant 25$; $-19 \leqslant l \leqslant 20$	$-24 \leqslant h \leqslant 22$; $-23 \leqslant k \leqslant 24$; $-19 \leqslant l \leqslant 20$
Number of reflections: measured/unique (N_1), R_{int}/with $I > 3\sigma(I)$ (N_2)	20645/2738, 0.0281/2738	123465/8227, 0.0326/7378
Refinement method	Full-matrix least squares based on	
Weighting scheme	$1/(\sigma^2(F) + 0.000036F^2)$	
Number of parameters	36	96
Extinction correction, coefficient	type 1, Lorentz [27], 0. 3640(50)	type 1, Lorentz [27], 0. 3460(40)
Flack parameter	0.583(3)	0.5828(19)
$R1/wR2$ based on N_1	0.0095/0.0123	0.0107/0.0122
$R1/wR2$ based on N_2	0.0095/0.0123	0.0094/0.0120
S	1.29	1.00
$\Delta\rho_{min}/\Delta\rho_{max}$, e/Å^3	−0.63/1.06	−0.85/1.32
Programs	CrysAlis, Jana2006	

Becker–Coppens model [27] for the mosaic spread (type I extinction, Lorentzian distribution) was chosen for each experiment. Principal crystallographic parameters and the X-ray-data-collection and structure-refinement statistics are summarized in Table 1. The atomic coordinates, site occupancies q, and equivalent isotropic displacement parameters are listed in Tables 2 and 3. Selected interatomic distances are given in Tables 4 and 5. The structural data were deposited at the Inorganic Crystal Structure Database (ICSD 431111, 431112).

RESULTS AND DISCUSSION

The atomic coordinates of the structure of the $GdFe_3(BO_3)_4$ single crystal, which was grown using a $K_2Mo_3O_{10}$-based flux [18], served as the starting model for the refinement of gadolinium iron borate at $T = 293$ and 90 K. The refinement revealed excessive occupancy factors for the Gd sites at both temperatures. Since the ionic radius of gadolinium is similar to that of bismuth ($r(Gd^{3+}) = 0.938$ Å, $r(Bi^{3+}) = 1.03$ Å) and is larger than the ionic radius of iron $r(Fe^{3+}) = 0.645$ Å [28], we hypothesized that bismuth impurity atoms found by chemical analysis are present in gadolinium sites. The refined formula of the compound based on the X-ray diffraction data is $Gd_{0.95}Bi_{0.05}Fe_3(BO_3)_4$ (Tables 2, 3). The crystal was a merohedral twin. The twin-component ratio at $T = 293$ is equal, within experimental error, to that at 90 K and is characterized by the Flack parameter of 0.583(3). The final values of the R factors are 0.95 and 0.94% for the structures at $T = 293$ and 90 K, respectively (Table 1).

The structure of the $Gd_{0.95}Bi_{0.05}Fe_3(BO_3)_4$ compound at 293 and 90 K is similar to the structures described in [18]. It is composed of layers alternating along the c axis. The first layer contains Fe and Gd(Bi) atoms and the second layer consists of triangular BO_3 groups. The triangles BO_3 are linked to Gd(Bi) and Fe atoms through oxygen vertices. Therefore, the structure determined at 293 K is composed of distorted $(Gd,Bi)O_6$ trigonal prisms, FeO_6 octahedra, and two

Table 2. Atomic coordinates, site occupancies (q), and equivalent isotropic displacement parameters for the $Gd_{0.95}Bi_{0.05}Fe_3(BO_3)_4$ structure at $T = 293$ K

Atom	x/a	y/b	z/c	q	U_{eq}, Å^2
Gd1 (3*a*)	0	0	0	0.95	0.007197(8)
Bi1(3*a*)	0	0	0	0.05	0.007197(8)
Fe1 (9*d*)	0.216576(9)	0.333333	0.333333	1	0.00509(1)
O1 (9*e*)	0.14423(5)	0.14423(5)	0.5	1	0.00671(6)
O2 (9*e*)	0.40883(6)	0.40883(6)	0.5	1	0.01194(10)
O3 (18*f*)	0.02540(4)	0.21261(5)	0.18268(5)	1	0.00810(6)
B1 (9*b*)	0	0	0.5	1	0.00526(11)
B2 (9*e*)	0.55248(7)	0.55248(7)	0.5	1	0.00619(11)

Table 3. Atomic coordinates, site occupancies (q), and equivalent isotropic displacement parameters for the $Gd_{0.95}Bi_{0.05}Fe_3(BO_3)_4$ structure at $T = 90$ K

Atom	x/a	y/b	z/c	q	U_{eq}, Å^2
Gd1 (3*a*)	−0.333416(2)	−0.333416(2)	0	0.95	0.002554(5)
Bi1 (3*a*)	−0.333416(2)	−0.333416(2)	0	0.05	0.002554(5)
Fe1 (3*a*)	0.115301(8)	0.115301(8)	0	1	0.00231(1)
Fe2 (6*c*)	−0.214058(7)	−0.549766(7)	0.341725(6)	1	0.00236(1)
O1 (3*b*)	0	−0.07817(4)	0.166667	1	0.00489(7)
O2 (6*c*)	−0.58320(3)	−0.27088(3)	0.13775(3)	1	0.00469(5)
O3 (6*c*)	−0.11921(4)	−0.30412(4)	−0.18013(4)	1	0.00431(5)
O4 (6*c*)	−0.14671(4)	−0.36260(4)	0.18507(4)	1	0.00417(5)
O5 (6*c*)	0.47561(4)	0.14527(4)	−0.15975(3)	1	0.00373(5)
O6 (3*b*)	0.18772(5)	0	−0.166667	1	0.00384(6)
O7 (6*c*)	−0.52354(4)	−0.53813(4)	−0.18570(4)	1	0.00433(6)
B1 (3*b*)	0.33207(7)	0	−0.166667	1	0.00340(10)
B2 (6*c*)	−0.44726(6)	−0.12054(6)	0.15593(5)	1	0.00366(9)
B3 (3*b*)	0	−0.22220(7)	0.166667	1	0.00357(10)

Table 4. Interatomic distances in the $Gd_{0.95}Bi_{0.05}Fe_3(BO_3)_4$ structure at $T = 293$ K

Gd1(3*a*) polyhedron		B1(9*b*) triangle	
Gd1–O3 × 6	2.368(1)	B1–O1 × 3	1.378(1)
$(Gd1–O3)_{av}$	2.368	$(B1–O3)_{av}$	1.378
Dispersion	0	Dispersion	0
Fe1(9*d*) polyhedron		**B2(9*e*) triangle**	
Fe1–O1 × 2	2.022(1)	B2–O2	1.373(1)
Fe1–O2 × 2	2.040(1)	B2–O3	1.372(1)
Fe1–O3 × 2	1.966(1)	$(B2–O3)_{av}$	1.372
$(Fe–O)_{av}$	2.009	Dispersion	0.001
Dispersion	0.056		

types of BO_3 triangles (Fig. 1). At 90 K two types of FeO_6 octahedra and three types of BO_3 groups are present.

At 293 K the rare earth ion in the $Gd_{0.95}Bi_{0.05}Fe_3(BO_3)_4$ structure (sp. gr. *R*32) is surrounded by six oxygen atoms of one type. The oxygen atoms occupy the vertices of the trigonal prism. The bases of this prism are parallel to the *ab* plane and are slightly rotated with respect to each other. All (Gd,Bi)–O distances have equal values (2.368(1) Å). The Gd(Bi) atoms, like the B1 atoms, lie on a threefold rotation axis parallel to the *c* axis (Figs. 2, 3). The distances from the Gd(Bi) atom to the six nearest iron atoms are equal and are 3.770 (1) Å.

At 90 K the Gd(Bi) atoms are surrounded by three types of oxygen atoms with a dispersion in the distances of 0.036 Å, resulting in a distortion of the $(Gd,Bi)O_6$ prism. The average (Gd,Bi)–O distance decreases only slightly with a decrease in the temperature. It should be noted that a similar dispersion in the Gd–O distances was found in [18]; however, the average distance was found to increase. The average dis-

tance from the Gd(Bi) atom to the six nearest iron atoms decreases to 3.765(1) Å. The dispersion in the distances is 0.114 Å. The Fe2 atoms are located at the shortest and longest distances from Gd(Bi) (Fig. 3).

At room temperature, the structure contains two independent boron sites (Fig. 2). Each boron atom is surrounded by three oxygen atoms in one plane with boron. The $B1O_3$ equilateral triangle is parallel to the *ab* plane, and the $B2O_3$ equilateral triangle is nearly parallel. At both temperatures, the $B1O_3$ triangles located above and below the $(Gd,Bi)O_6$ trigonal prisms are linked only to FeO_6 octahedra. The $B2O_3$ triangle is linked to two Fe atoms by one vertex. The other two vertices are linked to one Gd(Bi) atom and one Fe atom each.

In the structure of the low-temperature phase $Gd_{0.95}Bi_{0.05}Fe_3(BO_3)_4$, the number of independent boron atoms increases to three (Figs. 2, 4). In the $B1O_3$ triangles the average B1–O distances retain values characteristic of the structure at 293 K. However, the triangles are not exactly in the *ab* plane. The B2 site that is present in the structure at room temperature is split into B2 and B3 at 90 K (Fig. 4). The average B2–O distance is equal, within experimental error, to that determined at 293 K. The average distance in the $B3O_3$ isosceles triangle increases. The twofold axis in the *ab* plane, on which the B2 atom lies in the high-temperature structure, disappears. The oxygen triangle around B2 becomes scalene and is substantially distorted (the dispersion in the distances is 0.012 Å). In the other two triangles ($B1O_3$ and $B3O_3$), the B–O distances to the oxygen atoms almost equally increase. As a comparison, let us note that all average B–O distances in [18] are noticeably increased despite a decrease in the temperature. The oxygen environment of the B2 atom is also most distorted (the dispersion in the distances is 0.019 Å).

The $B2O_3$ triangles share one vertex with two $Fe(2)O_6$ octahedra, the second vertex is shared with the $(Gd,Bi)O_6$ prism and the $Fe(2)O_6$ octahedron, and the third vertex is shared with the $(Gd,Bi)O_6$ prism and the $Fe(1)O_6$ octahedron. The $B3O_3$ triangles are linked in a similar way to two $Fe(1)O_6$ octahedra by sharing one vertex, and are linked to $(Gd,Bi)O_6$ and $Fe(2)O_6$ by sharing the two other vertices (Figs. 4, 5).

The major structural elements in the crystal structure are helicoidal chains of edge-sharing FeO_6 octahedra (the Fe atoms belonging to one chain are symmetry-related by a threefold screw axis) running along the *c* axis. The chains are far apart from each other (i.e., the distances between the atoms from adjacent chains are larger than the distances between the atoms in the chain). At $T = 293$ K these chains are symmetry-related by a threefold rotation axis parallel to the *c* axis, with the Gd(Bi) and B1 atoms lying on this axis (Fig. 3). Each RO_6 polyhedron is located between three chains of FeO_6. The upper and lower vertices of the RO_6 polyhedron are shared with FeO_6 groups of the layers located above and below this polyhedron, respectively (Fig. 2). At room temperature, the distance between the nearest iron atoms in one chain (3.180(1) Å) is substantially smaller than the shortest distance (4.849(1) Å) between the iron atoms from adjacent chains (Fig. 3). This is indicative of the possible quasi-one-dimensional character of the interaction between the Fe^{3+} ions along the chains. The oxygen atoms O1 (linked to B1) and O2 (linked to B2) form an edge, which is shared by FeO_6 octahedra, resulting in the formation of a chain. The Fe–O1–Fe

Table 5. Interatomic distances in the $Gd_{0.95}Bi_{0.05}Fe_3(BO_3)_4$ structure at $T = 90$ K

Gd1(3*a*) polyhedron		B1(3*b*) triangle	
Gd1–O3 × 2	2.355(1)	B1–O5 × 2	1.379(1)
–O4 × 2	2.390(1)	–O6	1.378(1)
–O7 × 2	2.354(1)	$(B1–O)_{av}$	1.379
$(Gd1–O)_{av}$	2.366	Dispersion	0.001
Dispersion	0.036		
Fe1(3*a*) polyhedron		B2(6*c*) triangle	
Fe1–O1 × 2	2.044(1)	B2–O2	1.378(1)
–O3 × 2	1.959(1)	–O3	1.372(1)
–O6 × 2	2.010(1)	–O7	1.366(1)
$(Fe1–O)_{av}$	2.004	$(B2–O)_{av}$	1.372
Dispersion	0.085	Dispersion	0.012
Fe2(6*c*) polyhedron		B3(3*b*) triangle	
Fe2–O2	2.052(1)	B3–O1	1.374(1)
–O2	2.038(1)	–O4 × 2	1.378(1)
–O4	1.965(1)	$(B3–O)_{av}$	1.377
–O5	2.028(1)	Dispersion	0.004
–O5	2.020(1)		
–O7	1.973(1)		
$(Fe1–O)_{av}$	2.013		
Dispersion	0.087		

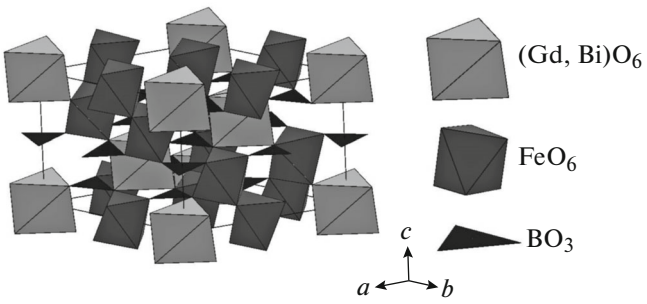

Fig. 1. Overall view of the $Gd_{0.95}Bi_{0.05}Fe_3(BO_3)_4$ structure.

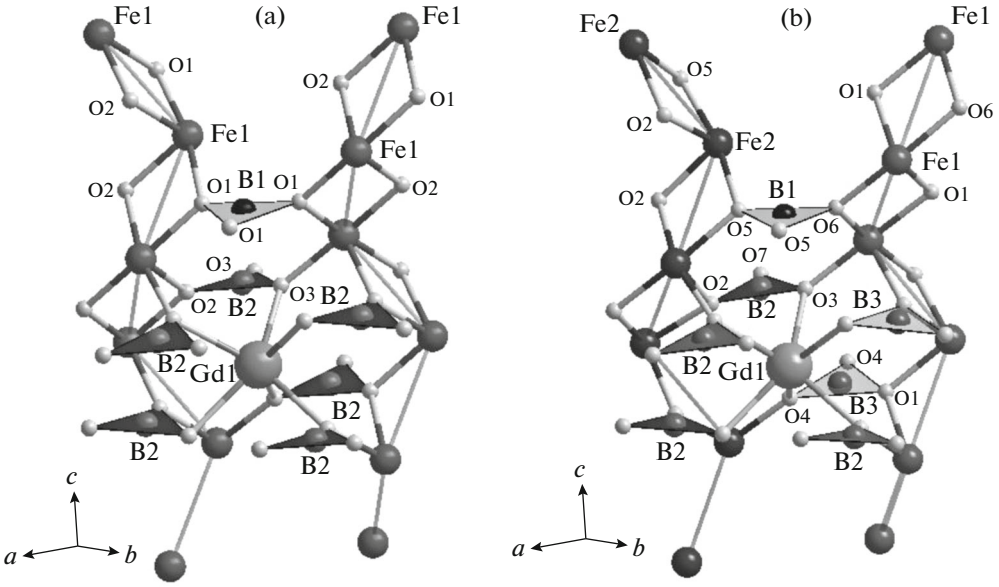

Fig. 2. Mutual arrangement of the chains of FeO_6 octahedra, $(Gd,Bi)O_6$ prisms, and BO_3 triangles in the $Gd_{0.95}Bi_{0.05}Fe_3(BO_3)_4$ structure at (a) 293 and (b) 90 K. The threefold axis passing through the B1 and Gd(Bi) atoms disappears with a decrease in the temperature. Two independent sites (Fe1 and Fe2) appear instead of one independent Fe1 site. The $B(2)O_3$ triangles are split into $B(2)O_3$ and $B(3)O_3$. The changes in the characteristic distances between the atoms and the angles between the chemical bonds are observed.

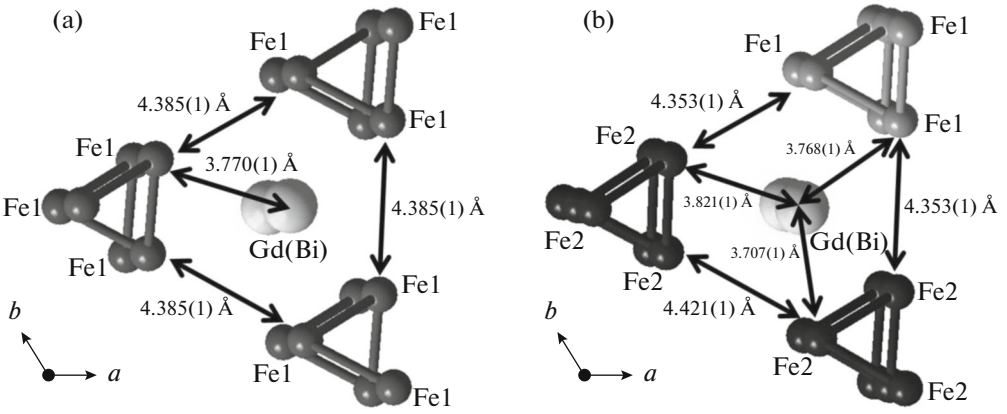

Fig. 3. Mutual arrangement of the chains of FeO_6 octahedra and Gd(Bi) atoms and the shortest distances between the atoms: (a) at 293 K the Gd(Bi) atoms are on a threefold axis parallel to the crystallographic *c* axis; (b) at 90 K the symmetry of the chains and the Gd(Bi) atoms is lower.

and Fe–O2–Fe angles have different values (103.7(1)° and 102.4(1)°, respectively).

At $T = 90$ K (sp. gr. $P3_121$), two nonequivalent iron sites (Fe1 and Fe2) with an occupancy ratio of 1 : 2 are present in the unit cell, giving rise to two types of iron chains. The helicoidal structure of the chains is retained (the symmetry with respect to the screw axis 3_1). However, the threefold rotation axis, which passes through the Gd(Bi) and B1 atoms and relates three chains at $T = 293$ K, is absent at $T = 90$ K. The Fe1 atoms, like in the structure at 293 K, are on a twofold axis lying in the *ab* plane, whereas the Fe2 atoms are shifted to a general position. One chain of Fe1 atoms and two chains of Fe2 atoms are formed instead of three Fe chains (Figs. 2, 3).

The average distance in the $Fe1O_6$ octahedra slightly decreases with a decrease in the temperature, whereas this distance in the $Fe2O_6$ octahedra increases compared to that observed at room temperature. Both octahedra are distorted due to an increase in the longest Fe–O distances and a decrease in the shortest Fe–O distances, the $Fe2O_6$ octahedron being characterized by a higher degree of distortion. An increase in the distortion of the iron polyhedra and an increase in

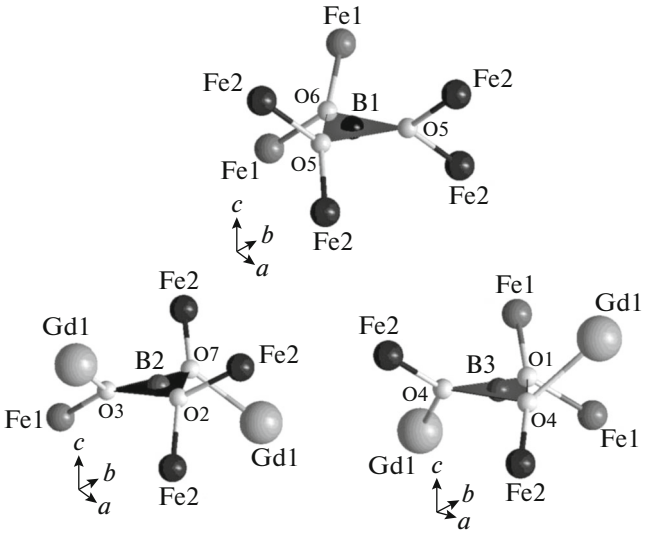

Fig. 4. Overall view of the atomic environment of the BO_3 triangles at 90 K.

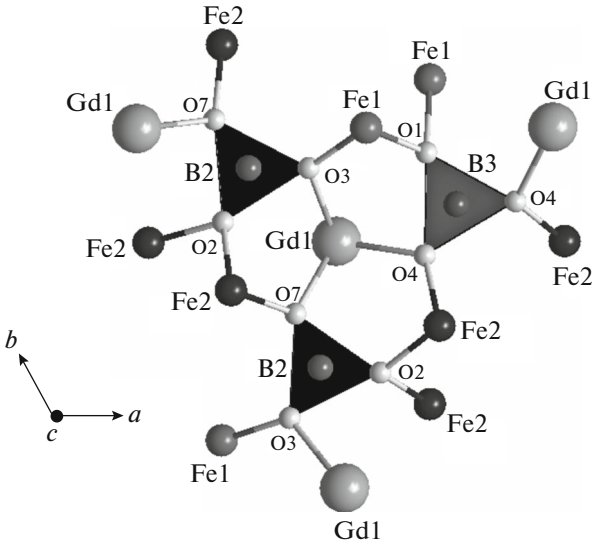

Fig. 5. Atomic environment of the upper base of the $(Gd,Bi)O_6$ prism at 90 K projected onto the *ab* plane.

the average distance in the $Fe2O_6$ octahedron were also observed for the compound studied in [18].

An analysis of the changes in the iron chains with a decrease in the temperature (Fig. 2) shows that the Fe1–Fe1 distances are decreased, whereas the Fe2–Fe2 distances are increased. In sp. gr. $P3_121$, the changes in the Fe–O–Fe angles in the chains are not equal. Thus, these angles are 0.13(1)° larger in the Fe2–O2–Fe2 chains and 0.31(1)° larger in the Fe2–O5–Fe2 chains. The oxygen atoms O2 and O5 are connected to the boron atoms B2 and B1, respectively. In the Fe1–O6–Fe1 chain, the angle remains unchanged within experimental error, whereas the angle in the Fe1–O1–Fe1 chain is noticeably smaller (by 1.07(1)°). The O6 atoms are linked to the B1 atoms; the O1 atoms are linked to the B3 atoms. There are also changes in the distances between the chains. Thus, the Fe1–Fe2 distances are shorter, whereas the Fe2–Fe2 distances are longer. Apparently, these changes are related to the displacements of the boron atom B2 and its environment with a decrease in the temperature, resulting in the disappearance of the twofold axis in the *ab* plane.

Therefore, a decrease in the temperature results in two types of nonequivalent iron chains with an occupancy ratio of 1 : 2 being present instead of three equivalent chains composed of octahedra of iron ions. Different crystal-chemical distortions give rise to two magnetic iron sublattices (Fe1 and Fe2), in which different types of magnetic ordering occur upon further cooling below the Néel temperature $T_N \approx 38$ K [20].

CONCLUSIONS

Single crystals of $Gd_{0.95}Bi_{0.05}Fe_3(BO_3)_4$ were studied by X-ray diffraction at 293 and 90 K. At both temperatures, the crystals have a trigonal symmetry. It was found that the first-order phase transition leads to the change in sp. gr. $R32 \rightarrow P3_121$. In the low-symmetry structure, the changes in the bond lengths in the $(Gd,Bi)O_6$ prisms, $B2O_3$ triangles, and FeO_6 octahedra are not equal. Two types of nonequivalent chains composed of FeO_6 octahedra are formed instead of one type of iron chains. Apparently, the presence of two structural sites of iron (Fe1 and Fe2) is responsible for the formation of two magnetic iron sublattices, in which different types of magnetic ordering occur upon further cooling below the Néel temperature $T_N \sim 38$ K.

ACKNOWLEDGMENTS

This study was performed using the equipment of the Center of Collective Use of the Shubnikov Institute of Crystallography of the Russian Academy of Sciences and it was supported by the Ministry of Education and Science of the Russian Federation (Project RFMEFI62114X0005) and in part by the Russian Foundation for Basic Research (Grant nos. 14-02-00483 and 14-02-00307) and the Federal Program on Support of Leading Scientific Schools (Grant no. NSh-6617.2016.5).

REFERENCES

1. A. N. Vasil'ev and E. A. Popova, Fiz. Nizk. Temp. (Kiev) **32** (8/9), 968 (2006).
2. A. M. Kadomtseva, V. Yu. Ivanov, L. N. Bezmaternykh, et al., Fiz. Nizk. Temp. (Kiev) **36** (6), 640 (2010).

3. J.-C. Joubert, W. B. White, and R. Roy, Appl. Cryst. **1**, 318 (1968).
4. J. A. Campá, C. Cascales, E. Gutiérrez-Puebla, et al., Chem. Mater. **9**, 237 (1997).
5. L. N. Bezmaternykh, S. A. Kharlamova, and V. L. Temerov, Crystallogr. Rep. **49** (5), 855 (2004).
6. A. D. Balaev, L. N. Bezmaternykh, and I. A. Gudim, J. Magn. Magn. Mater. **258–259**, 532 (2003).
7. W. A. Dollase and R. J. Reeder, Am. Mineral. **71**, 163 (1986).
8. Y. Hinatsu, Y. Doi, K. Ito, et al., J. Solid State Chem. **172**, 438 (2003).
9. D. Fausti, A. A. Nugroho, P. H. M. van Loosdrecht, et al., Phys. Rev. B **74**, 024403 (2006).
10. P. Fischer, V. Pomjakushin, D. Sheptyakov, et al., J. Phys.: Condens. Matter **18**, 7975 (2006).
11. M. N. Popova, J. Magn. Magn. Mater. **321**, 716 (2009).
12. R. Z. Levitin, E. A. Popova, R. M. Chtsherbov, et al., JETP Lett. **79** (9), 423 (2004).
13. A. G. Gavrilyuk and S. A. Kharlamova, JETP Lett. **80** (6), 426 (2004).
14. A. G. Gavriliuk and S. A. Kharlamova, J. Phys.: Condens. Matter **17**, 1 (2005).
15. S. A. Kharlamova and S. G. Ovchinnikov, JETP Lett. **101** (6), 1098 (2005).
16. I. S. Lyubutin, A. G. Gavrilyuk, V. V. Struzhkin, et al., JETP Lett. **84** (9), 518 (2006).
17. E. L. Belokoneva, L. I. Al'shinskaya, and M. A. Simonov, Zh. Strukt. Khim. **20** (3), 542 (1979).
18. S. A. Klimin, D. Fausti, A. Meetsma, et al., Acta Crystallogr. B **61**, 481 (2005).
19. A. V. Malakhovskii, V. V. Sokolov, A. L. Sukhachev, et al., Phys. Solid State **56** (10), 2056 (2014).
20. K. V. Frolov, I. S. Lyubutin, E. S. Smirnova, et al., J. Alloys Compd. **671**, 545 (2016).
21. L. M. Volkova and D. V. Marinin, J. Supercond. Nov. Magn. **34**, 2161 (2011).
22. A. P. Dudka, I. A. Verin, and E. S. Smirnova, Crystallogr. Rep. **61** (4), 682 (2016).
23. A. Dudka, J. Appl. Crystallogr. **43** (6), 1440 (2010).
24. A. P. Dudka, Crystallogr. Rep. **50** (6), 1068 (2005).
25. *CrysAlis system. Version 1.171.37.31* (release 14-01-2014 CrysAlis171.NET).
26. V. Petricek, M. Dusek, and L. Palatinus, Z. Kristallogr. B **229** (5), 345 (2014).
27. P. J. Becker and P. Coppens, Acta Crystallogr. A **30**, 129 (1974).
28. R. D. Shannon, Acta Crystallogr. A **32**, 751 (1976).

Translated by T. Safonova